Article

Journal of the Brazilian Chemical Society

https://dx.doi.org/10.21577/0103-5053.20230169

J. Braz. Chem. Soc. **2024**, *35*, 5, e-20230169, 1-13

Effect of the Synthesis Parameters on the Physicochemical Properties and Photocatalytic Performance of Nb_2O_5 to Water Treatment and H_2 Production

Marlete A. Souza,[a] *Marcela P. Bernardo,*[a] *Higor O. Alves,*[a] *Cleiton P. M. Silva,*[a] *Antônio Otávio T. Patrocínio*[a] *and Osmando F. Lopes*[*,a]

[a]*Instituto de Química, Universidade Federal de Uberlândia (IQUFU), Av. João Naves de Ávila, 2121, Bairro Santa Mônica, 38400-902 Uberlândia-MG, Brazil*

Nb_2O_5 is a promising photocatalyst for degradation of organic pollutants and production of H_2 (renewable and green fuel) from water is an alternative to overcome environmental and energy concerns. Therefore, the effect of Nb precursor and synthesis method on the Nb_2O_5 physical-chemical properties and photocatalytic performance were investigated in this work. X-ray diffraction and Raman spectroscopy results showed that synthesis parameters had a significant impact on the structural properties of the materials obtained. The synthesis parameters were able to tune Nb_2O_5 crystalline phase, morphology and specific surface area. Nb_2O_5 sample obtained by hydrothermal method resulted in materials with smaller size and homogeneous particles compared to the other samples, which resulted in a higher specific surface area (200 $m^2 g^{-1}$) and surface hydroxylation. Nb_2O_5 samples were active to promote both the degradation of Rhodamine B and amiloride, the specific surface area and surface hydroxylation play a key role in the performance of the materials. The most active sample for organic pollutant degradation was also active in H_2 production, additionally, the decoration with Pt nanoparticles increased its performance. This work describes the effect of synthesis parameters of Nb_2O_5 on its photocatalytic properties and demonstrates the potential application of this material in heterogeneous photocatalysis.

Keywords: niobium pentoxide, hydrothermal method, organic pollutant degradation, water splitting

Introduction

Water is one of the most valuable and crucial natural resources for sustaining life on Earth.[1] While approximately 70% of the Earth's surface is covered with water, only 2.5% of it is considered safe for consumption. The contamination due to improper disposal of domestic, industrial, and agricultural effluents is exacerbating this situation,[2,3] highlighting the need for strategies to treat and reuse water.[4] Additionally, the increasing demand for energy from non-renewable sources and its contribution to air pollution, global warming and climate changes are a major environmental and energy concern worldwide. Then, the development of methods to obtain energy in a clean and sustainable way becomes imperative. Therefore, solar light as a primary energy resource stands out for its advantages in terms of spread availability and accessibility in an inexhaustible and inexpensive way around the world.[5] The possibility to convert light into valuable solar fuels from water is a promising approach to provide clean energy and, at the same time, contribute to mitigate the global warming effect.[6]

Heterogeneous photocatalysis is a promising method for treating water effluents (organic pollutant degradation) as well as for renewable energy production, e.g., hydrogen production.[7,8] This method stands out due to its low cost and high efficiency, which can be conducted under solar radiation. A wide range of metal oxide semiconductors have been applied as photocatalysts because they have interesting optical and electrical properties as well as high surface areas, which enhance their performance in photocatalytic applications.[9] TiO_2 and ZnO are the benchmark photocatalysts to promote organic pollutant degradation and H_2 production.[10-15] However, these semiconductors face several challenges for practical applications, such as fast charge recombination and low

*e-mail: osmando@ufu.br
Editor handled this article: Izaura C. N. Diógenes (Associate)
This manuscript is part of a series of publications in the Journal of the Brazilian Chemical Society by young researchers who work in Brazil or have a solid scientific connection with our country. The JBCS welcomes these young investigators who brighten the future of chemical sciences.

stability. For this reason, many other semiconductor classes have been studied, for example, the perovskite materials based on Ti ($BaTiO_3$, $SrTiO_3$, $CaTiO_3$).[16,17] Among a variety of photocatalysts, niobium pentoxide (Nb_2O_5) has been investigated owing to its suitable electronic and morphological properties for light-driving reactions and due to its characteristics very similar to TiO_2.[18-20] Nb_2O_5 exhibits more than 15 different structural configurations, and its oxides exhibit different properties depending on the crystalline phase, preparation and desired application.[21] Thus, Nb_2O_5 is a very complex material to evaluate, and its understanding is still noticeably insufficient.[22-24]

Some studies have shown that Nb_2O_5 samples exhibit a remarkable photocatalytic performance. For example, Su *et al.*[25] developed a modified sol-gel with a calcination step at 550 ºC to obtain Pt over 2D Nb_2O_5 nanoparticles. This material presented a high photoactivity for the reaction of phenylacetylene hydrogenation. Guo and co-workers[26] developed a two-step synthesis route (hydrothermal and calcination) to obtain N-doped Nb_2O_5 microsphere. They observed that N doping increased the charge carrier lifetime of Nb_2O_5 and resulted in higher photocatalytic performance for pesticide degradation.[27] Ücker *et al.*[28] evaluated the photocatalytic performance of Fe inserted in Nb_2O_5 obtained by microwave-assisted hydrothermal synthesis. They stated that Fe insertion in the Nb_2O_5 increased the charge carrier lifetime and resulted in the improvement of photocatalytic performance for Rhodamine B degradation. Cui *et al.*[29] reported a strategy to improve the photocatalytic performance of the commercial TiO_2 (Degussa P25) by addition of Nb_2O_5. The composite was obtained by annealing a mixture of TiO_2 and Nb_2O_5 at 550 ºC. The samples were applied in the photodegradation of 1,4-dichlorobenzene; it was necessary 10 h to promote the degradation of only 60% of the organic pollutant. Peng *et al.*[30] proposed the preparation of a ternary $Ag/Nb_2O_5@Nb_2CT_x$ nanohybrid material through a hydrothermal method followed by an Ag photodeposition. The composite materials were applied as photocatalyst for hydrogen evolution reaction. Despite the high Nb_2O_5's photoactivity for organic pollutants degradation and hydrogen evolution reaction, Nb_2O_5 samples are generally obtained by a calcination step in a high temperature (> 500 ºC) that results in material with a low specific surface area and density of active sites, which is a key property for application in heterogenous process.[31] Additionally, Nb_2O_5 is a very complex material due to its many phases and polymorphs, and many works reported contradictory or inconsistent information.[22,23] Therefore, obtaining Nb_2O_5 nanoparticles with controlled particle size, morphology, specific surface area and crystalline phase is essential to advance the application of this material.[24]

Therefore, the main objective of this work is to investigate the effect of synthesis parameters (different synthesis methods and niobium precursor) on the physical-chemical properties of Nb_2O_5 and its photocatalytic performance in the degradation of organic pollutants and H_2 production. The photocatalytic performance of the Nb_2O_5 samples and the degradation mechanisms involved reaction were evaluated using Rhodamine B (dye) and amiloride (drug) as probes. Nb_2O_5 modified with Pt nanoparticles was also applied as a photocatalyst for H_2 production.

Experimental

Nb_2O_5 synthesis

In order to investigate the precursor effect on the Nb_2O_5 synthesis by oxidant peroxo method with crystallization by hydrothermal conditions, two different precursors were employed: niobium ammonium oxalate ($NH_4NbO(C_2O_4)_2(H_2O)_2]nH_2O$) and commercial niobium oxide (Nb_2O_5, optical grade, > 99.8%) both provided by Companhia Brasileira de Metalurgia e Mineração (CBMM), Brazil. In both cases, it was added 5 mmol of the Nb precursor in 100 mL of distillated water. To that suspension, it was added 6.7 mL of hydrogen peroxide (H_2O_2) at the molar ratio of 1:10 of Nb:H_2O_2, according to the peroxide oxidation synthesis.[20,32] The addition of H_2O_2 to Nb_2O_5 generated the formation of the niobium peroxocomplex, which was confirmed by the formation of a yellow solution. This solution was added to teflon jar and hydrothermally treated at 120 °C for 18 h. After the reaction, the material was washed twice with distillated water and once with isopropanol. The obtained material was dried at 50 °C for 5 h. The sample obtained from the niobium ammonium oxalate precursor was named Nb_2O_5 A.H. and the sample synthetized using commercial Nb_2O_5 was labeled as Nb_2O_5 C.H. To investigate the effect of the crystallinity degree of Nb_2O_5, the niobium ammonium oxalate precursor was annealed to obtain a material with high crystallinity and orthorhombic crystalline phase.[33] To achieve this aim, 2 g of this precursor were annealed at 600 °C for 2 h, at 5 °C min^{-1}. This material was named Nb_2O_5 A.C. The samples were labeled according to the synthesis method and precursor employed as can be seen in the Table 1.

Characterization

The Nb_2O_5 powder samples synthesized were characterized by X-ray diffraction (XRD) on a Shimadzu XRD 6000 diffractometer (Kyoto, Japan) using Ni-filtered Cu Kα radiation (λ = 1.5405 Å). The XRD patterns were

Table 1. Nb_2O_5 samples label according to the preparation conditions

Sample	Precursor	Synthesis method
Nb_2O_5 A.H.	ammonium niobium oxalate	hydrothermal
Nb_2O_5 A.C.	ammonium niobium oxalate	annealing
Nb_2O_5 C.H.	commercial Nb_2O_5	hydrothermal
Nb_2O_5 C	commercial Nb_2O_5	no treatment

taken over the 2θ range of 10-70 degrees with a scan speed of 1 degree min^{-1}; Fourier transform infrared (FTIR) analyses were performed on a PerkinElmer Frontier spectrometer (Massachusetts, United States) using spectral resolution of 4 cm^{-1} in the range of 4000-400 cm^{-1}. Raman spectroscopy analysis was performed at Horiba LabRAM HR Evolution (Kyoto, Japan), with laser excitation of 532 nm, potential filter 3.2%, 600 lines mm^{-1} and 6 scans accumulation. The specific surface area of the samples was estimated by N_2 physisorption analysis at 77 K in the Micrometrics ASAP 2000 equipment (Norcross, Georgia, USA) applying BET (Brunauer-Emmett-Teller) model. Prior to the analyses, the samples were pre-treated (degasification) by heating at 80 °C under vacuum until reaching a degassing pressure lower than 10 μmHg.

Scanning electron microscopy (SEM) was conducted on a TESCAN microscope (Brno, Czech Republic) running at 5 kV. X-ray dispersive energy spectroscopy (EDX) was used to determine qualitatively the elemental composition of the Nb compounds. Transmission electronic microscopy (TEM) was conducted on Hitachi HT7700 microscope (Kyoto, Japan). Diffuse reflectance spectra (DRS) in the ultraviolet-visible region were recorded between 200 and 800 nm, at room temperature, using a UV-Vis Shimadzu UV-2600 (Kyoto, Japan) with sphere of integration (ISR-2600 Plus) operated in diffuse reflectance mode to determine the band gap of the materials.

Evaluation of Nb_2O_5 photoactivity

The photocatalytic performance of the Nb_2O_5 samples was evaluated using two different organic contaminants as probes, Rhodamine B dye (RhB, Sigma-Aldrich, Saint Louis, Missouri, USA) and amiloride drug (Sigma-Aldrich, Saint Louis, Missouri, USA). The photoactivities were studied under UV radiation using Lamps Phillips (Eindhoven, Netherlands) TUV, 15 W and maximum intensity at 254 nm, with medium intensity of irradiance of 40 mW m^{-2} in a photoreactor at 18 °C. To perform the photocatalytic tests, 25 mg of each photocatalyst were dispersed in 50 mL of aqueous RhB (5 mg L^{-1}, pH = 6.3) or amiloride (10 mg L^{-1}, pH = 5.5). At regular time intervals, the samples were collected and analyzed in a UV-Vis spectrophotometer Evolution 201/220, ThermoFisher Scientific (Massachusetts, USA). RhB and amiloride were monitored by its maximum absorption peak at 532 and 286 nm, respectively. The samples in dye or in drug solution were kept in the dark for 12 h before the photocatalytic experiment to reach the adsorption-desorption equilibrium.

The organic pollutant photodegradation mechanism driven by the Nb_2O_5 photocatalysts was investigated by using scavengers of active species. This experiment consisted of adding reactive species scavengers directly to the samples containing RhB dye. In this procedure, *tert*-butanol (*t*-BuOH, 100 μmol L^{-1}), ethylenediaminetetraacetic acid (EDTA, 50 μmol L^{-1}), or benzoquinone (BQ, 50 μmol L^{-1}) were added as scavengers for radical $^{\bullet}OH$ radicals, valence band (VB) photogenerated holes (h^+), and conduction band (CB) photogenerated electrons (e^-), respectively.[34,35]

Photocatalytic production of H_2

The sample Nb_2O_5 A.H. presented the highest photoacatalytic performance for organic pollutant degradation, so it was chosen to be used as catalyst for H_2 production. To improve the sample's photocatalytic performance, it was modified by the deposition of Pt nanoparticles on the surface using a photodeposition method, largely employed in the literature.[36-38] Pt modification was carried out by the addition of 1 mL of 2.09×10^{-3} mol L^{-1} H_2PtCl_6 aqueous to 40 mg of the Nb_2O_5 A.H. suspended in 20% v/v methanol/water. The mixture was stirred for 24 h under UV irradiation (315-380 nm, 24 W), and afterward, the solid was filtered, washed with deionized water, and dried at 80 °C. The final metal weight percentage in relation to the sample was 1% wt.

The photocatalytic performance of the Nb_2O_5 to produce H_2 were carried out at 25 °C in a septum-sealed 18 mL borosilicate double-walled reactor connected to a thermostatic bath. The photocatalysts (5 mg) were added to methanol/water solution (20% v/v) and kept under magnetic stirring. The reactor was purged with argon for 10 min and then exposed to irradiation of xenon lamp (300 W, $\lambda > 320$ nm) placed in a 67011 Newport lamp house connected to a 69911 source, with 120 mW cm^{-2} of irradiance during 8 h. The irradiance was measured using Powermeter Newport 1916-R (Andover, Massachusetts, US). At regular time interval, 0.5 mL gas samples were collected from the headspace of the reactor and analyzed by gas chromatography using a Clarus 580, PerkinElmer (Massachusetts, US) equipped with two columns (Porapak N 2 mm and molecular sieve) and one detector of thermal conductivity. The measurements were performed at 120 °C on the injector and 150 °C on the detector, with

thermal ramp of 35-120 °C. Ar was used as carrier gas at 30 mL min^{-1}.[37]

Results and Discussion

Microstructural characterization

The structural and phase formation analysis in the crystalline lattice of the Nb_2O_5 samples synthetized were evaluated by XRD, as can be seen in Figures 1a-1b. It can be verified that the Nb_2O_5 samples are crystalline. Nb_2O_5 A.H. showed characteristic peaks of the pseudohexagonal (TT) crystalline phase of Nb_2O_5 (JCPDS: 28-317).[20,32,39] The TT-Nb_2O_5 is a metastable phase and it can be stabilized due to the presence of impurities at the crystal lattice.[32] This sample exhibits also two large diffraction peaks at 12 and 26 degrees, related to niobium oxide hydrated ($Nb_2O_5.nH_2O$).[20,40] On the other hand, the sample Nb_2O_5 A.C., obtained by the annealing of the ammoniacal complex precursor, exhibits characteristic peaks related to the orthorhombic (T) crystalline phase of Nb_2O_5 (JCPDS No. 00-027-1313).[33] The sample Nb_2O_5 A.C. showed peaks with a higher intensity and well-shaped in comparison to Nb_2O_5 A.H., because the calcination in high temperatures provides enough thermal energy for the material's crystallization. Therefore, when niobium ammonium oxalate was used as precursor, the synthesis method (hydrothermal or calcination) had significant impact on the structural materials properties.

The XRD patterns for commercial Nb_2O_5 (Nb_2O_5 C) exhibit characteristic peaks of the orthorhombic (T) and monoclinic (H) crystalline phases (JCPDS No. 01-72-1121), presenting a phase mixture (Figure 1b) that agrees with the literature.[41] The hydrothermal treatment using commercial Nb_2O_5 as precursor does not result in significant modifications of the XRD profile of the sample Nb_2O_5 C.H. Therefore, the hydrothermal treatment did not show a significant effect at the crystalline structure of the sample Nb_2O_5 C.H. This could be related to the high stability and insolubility of the commercial Nb_2O_5, for example, it was required a thermal treatment higher than 900 ºC to modify the structure of the Nb_2O_5 C sample.[42,43]

Figure 2a shows the FTIR spectra of the Nb_2O_5 samples. All the samples present bands in the region of 1000-500 cm^{-1} which are characteristics of Nb–O bonding. The bands around 718 and 500 cm^{-1} are related to Nb=O stretch and angular vibrations of Nb–O–Nb.[44] The sample Nb_2O_5 A.H. shows bands around 1720-1410 cm^{-1} attributed to C–O and C=O that can be related to oxalate and carbonyl groups from the synthesis residues. The presence of these residues may be responsible for the stabilization of the pseudohexagonal

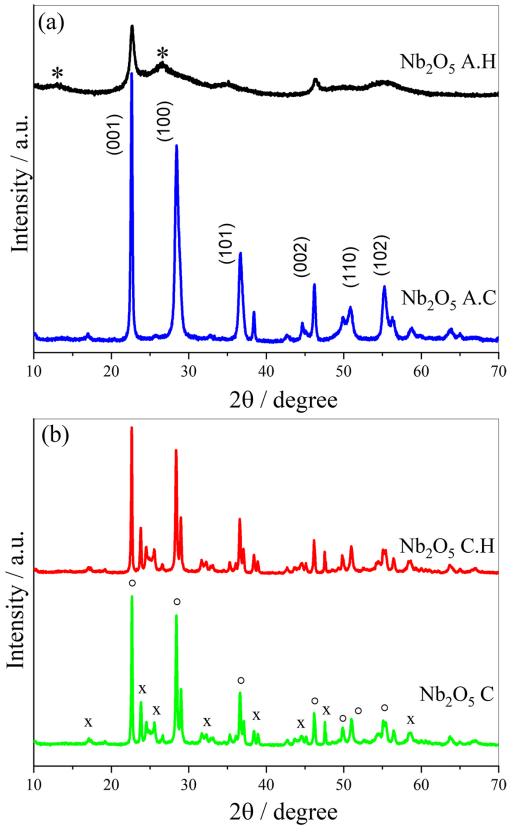

Figure 1. XRD patterns of Nb_2O_5 samples obtained by different methods and using as precursor: (a) ammonium oxalate complex of niobium, where * is referent to $Nb_2O_5.nH_2O$ and the indexed peaks are referent to the TT- Nb_2O_5, JCPDS: 28-317 phase; (b) commercial Nb_2O_5, where X and ° represents the crystalline phases, T-Nb_2O_5 and H-Nb_2O_5, respectively.

metastable phase of Nb_2O_5. Weissman *et al.*[45] proposed that niobium atoms at TT-Nb_2O_5 phase are in more symmetric Wyckoff positions, which can produce an open unit cell, with a more evenly spaced position to accommodate impurities and defects.[20,45-47] This sample also presents centered bands around 3357 cm^{-1} that can be attributed to hydroxyl groups adsorbed on the surface of the sample. It is worth pointing out that the presence of hydroxyl groups at the surface of the semiconductors may affect positively the photocatalytic performance of the sample, because the photogenerated holes may oxide the hydroxyl groups and generate hydroxyl radicals (•OH) that promote the degradation of organic pollutants.[48-50] This happens because the adsorption of the hydroxyl group can decrease the reduction potential to convert it in hydroxyl radicals. The Nb_2O_5 A.C. sample did not exhibit the presence of IR bands related to the carboxyl and hydroxyl groups; it means that the calcination step at high temperature was efficient to remove the synthesis residues. Additionally, the hydrothermal treatment of commercial Nb_2O_5 was not enough to cause significant modification in its functional groups on the samples surface.

The Nb_2O_5 samples were characterized by Raman spectroscopy (Figure 2b). The Nb_2O_5 A.H. sample shows large and less defined peaks in comparison to the other samples, which can be related to TT-Nb_2O_5 phase. The peaks around 685 and 228 cm^1 are attributed to octahedral coordination of NbO_6 and to vibrational modes of Nb–O–Nb bonding, respectively. NbO_6 of low distortion is characteristic of samples with low crystallinity degree.[51,52] The sample Nb_2O_5 A.C. showed sharper peaks and a displacement of the main peak from 685 to 700 cm^{-1}, related to the crystalline phase changes. The small peak at 890 cm^{-1} may be attributed to low concentrations of the surface groups Nb=O. These observed modifications reinforce the conclusion that the calcination promoted the formation of Nb_2O_5 on the orthorhombic phase, as observed by XRD results. The commercial Nb_2O_5 exhibits defined peaks and additional peaks around 900 and 997 cm^{-1}, attributed to the symmetric elongation mode and antisymmetric mode of Nb=O terminal bonds, respectively.[51,52] These peaks may be related to the monoclinic phase of Nb_2O_5, in agreement with XRD results. The hydrothermal treatment on commercial Nb_2O_5 resulted in peaks more sharp and intense, which indicates the increase of structural ordering of the sample, caused by the hydrothermal treatment.

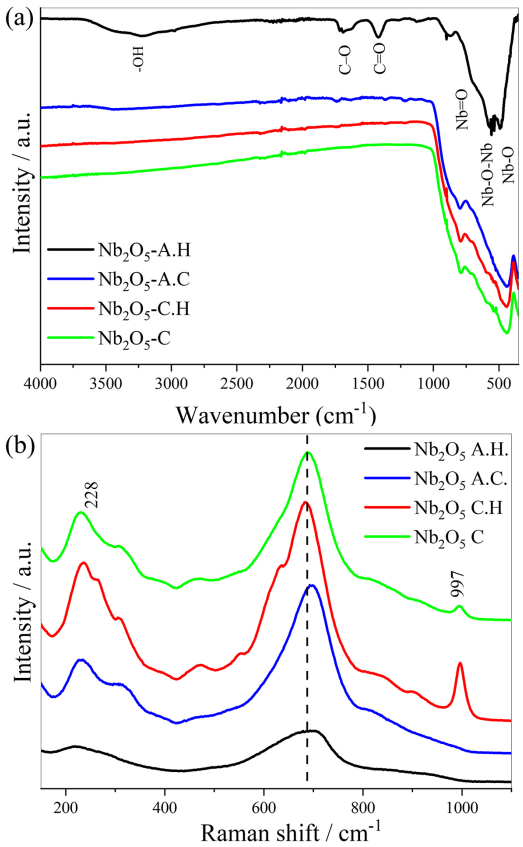

Figure 2. (a) FTIR-ATR and (b) Raman spectra for Nb_2O_5 samples obtained by different synthesis methods and different precursors.

The electronic properties of the Nb_2O_5 samples were characterized by ultraviolet-visible diffuse reflectance spectroscopy (UV-Vis DRS) (Figure S1, Supplementary Information (SI) section). The band gap energies of the synthetized samples were determined applying the Tauc equation to the DRS data:

$$(\alpha h\nu)^{\frac{1}{n}} = A\left(hf - E_g\right) \quad (1)$$

where, α, h, f, E_g, A are the absorption coefficient, Planck's constant, radiation frequency, band gap energy and a constant, respectively. The n constant depends on the nature of the electron transition and is equal to 1/2 or 2 for the direct and indirect transition band gaps, respectively. Nb_2O_5 exhibits an indirect transition band gap. Tauc plots with the respective value of band gap energy for all Nb_2O_5 samples can be observed in Figure 3. Nb_2O_5 A.H. sample exhibited the higher value for band gap energy in comparison to the other samples, around 3.3 eV. The other samples exhibited values of band gap around 3.1 eV, which indicates that the orthorhombic and monoclinic phases of Nb_2O_5 presented a band gap value slightly lower than the pseudohexagonal phase. The values of the band gap and the observed tendency agree with other studies.[53,54] Because the Nb_2O_5 A.H. sample presented a band gap energy higher than the other samples, it can result in band edge levels with higher redox potential to promote the reactions of organic pollutant degradation and hydrogen evolution.[54-56]

Specific surface area, pore size and pore volume average were determined from nitrogen adsorption/desorption isotherms, Table 2. Figure 4 shows the N_2 adsorption-desorption isotherms of Nb_2O_5 samples. The N_2 adsorption-desorption isotherms of the three samples exhibit typical type IV with hysteresis loop type H2 of International Union of Pure and Applied Chemistry (IUPAC) classification, which is associated with capillary condensation taking place in mesopores materials. Table 2 shows that Nb_2O_5 A.H. sample exhibits a specific surface area (SSA) value around 9 and 20 times higher than Nb_2O_5 A.C. and Nb_2O_5 C samples, respectively. The same trend is observed when evaluating the total pore volume. All samples exhibit average pore size in the range of 2.6 to 6.7 nm, which can be classified as mesoporous materials. Additionally, the samples do not exhibit a plateau at high-pressure values, suggesting the presence of a wider pore size distribution.

The morphology of the synthetized samples was characterized by SEM, as can be seen in Figure 5. All the synthetized samples exhibit particles with spherical morphology. Nb_2O_5 A.H. exhibited nanometric particles with homogenous size and morphology, which indicates

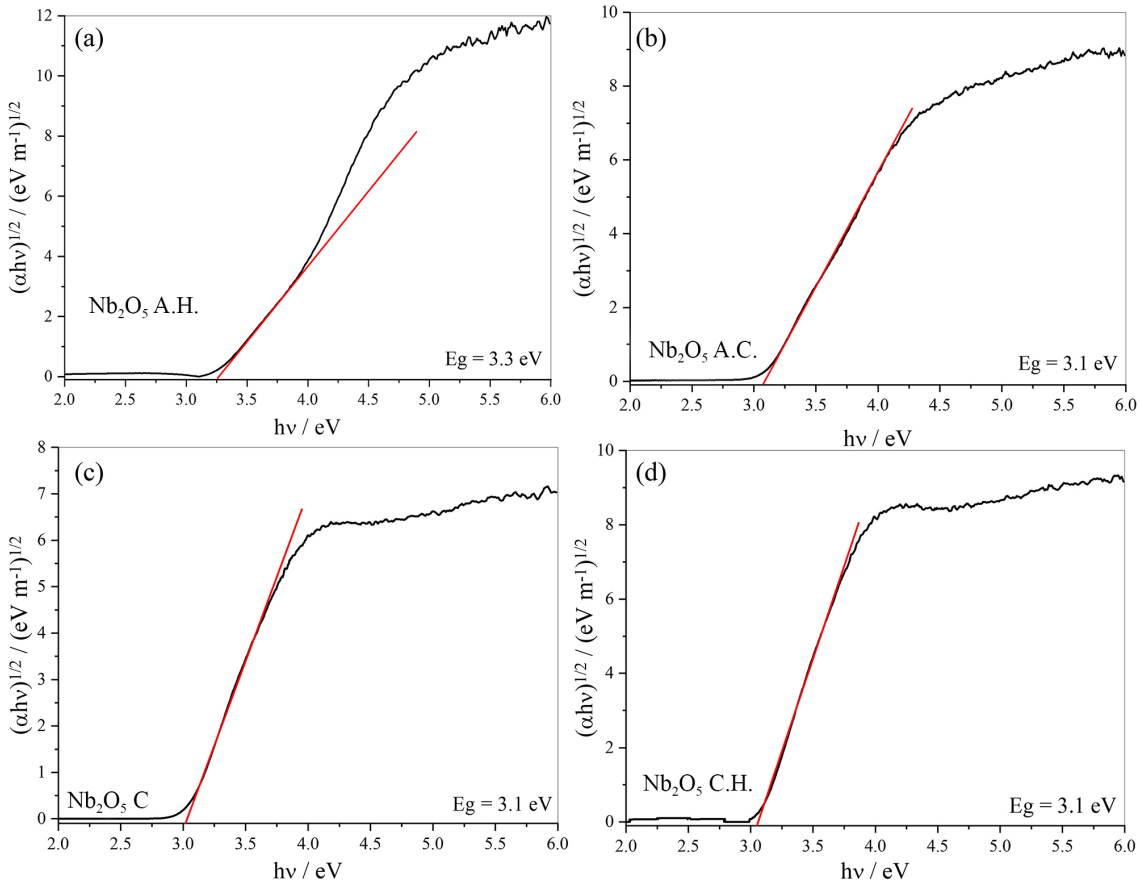

Figure 3. Tauc plot obtained from UV-Vis diffuse reflectance spectroscopy data of the samples: (a) Nb_2O_5 A.H., (b) Nb_2O_5 A.C., (c) Nb_2O_5 C and (d) Nb_2O_5 C.H.

Table 2. Band gap values obtained by Tauc equation and N_2 physisorption data of Nb_2O_5 samples

Sample	Band gap / eV	SSA / ($m^2 g^{-1}$)	Pore volume / ($cm^3 g^{-1}$)	Pore size / nm
Nb_2O_5 A.H.	3.3	267	0.55	4.7
Nb_2O_5 A.C.	3.1	29	0.09	6.7
Nb_2O_5 C.H.	3.1	–	–	–
Nb_2O_5 C	3.1	13	0.02	2.6

SSA: specific surface area.

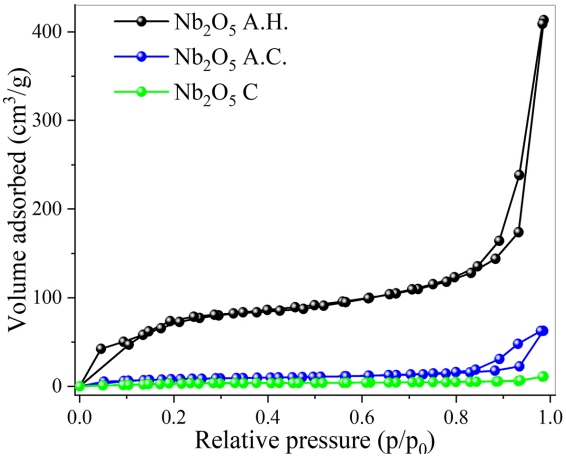

Figure 4. N_2 adsorption-desorption isotherms of Nb_2O_5 samples.

that hydrothermal method was efficient (Figure 5a). However, the calcination of ammonium oxalate complex of niobium resulted on the formation of micrometrics particles agglomerated, caused by the particles calcination at high temperatures (Figure 5b). It agrees with the specific surface area of Nb_2O_5 A.H. and Nb_2O_5 A.C. samples, where the precursor calcination resulted in a material with specific surface area around 9 times smaller than the samples obtained by the hydrothermal route.[33] On the other hand, the comparison between Nb_2O_5 C sample (Figure 5c) with Nb_2O_5 C.H (Figure 5d) did not show any significant modification caused by the hydrothermal treatment.[57]

Nb_2O_5 A.H. sample was characterized by transmission electron microscopy and compared with the sample

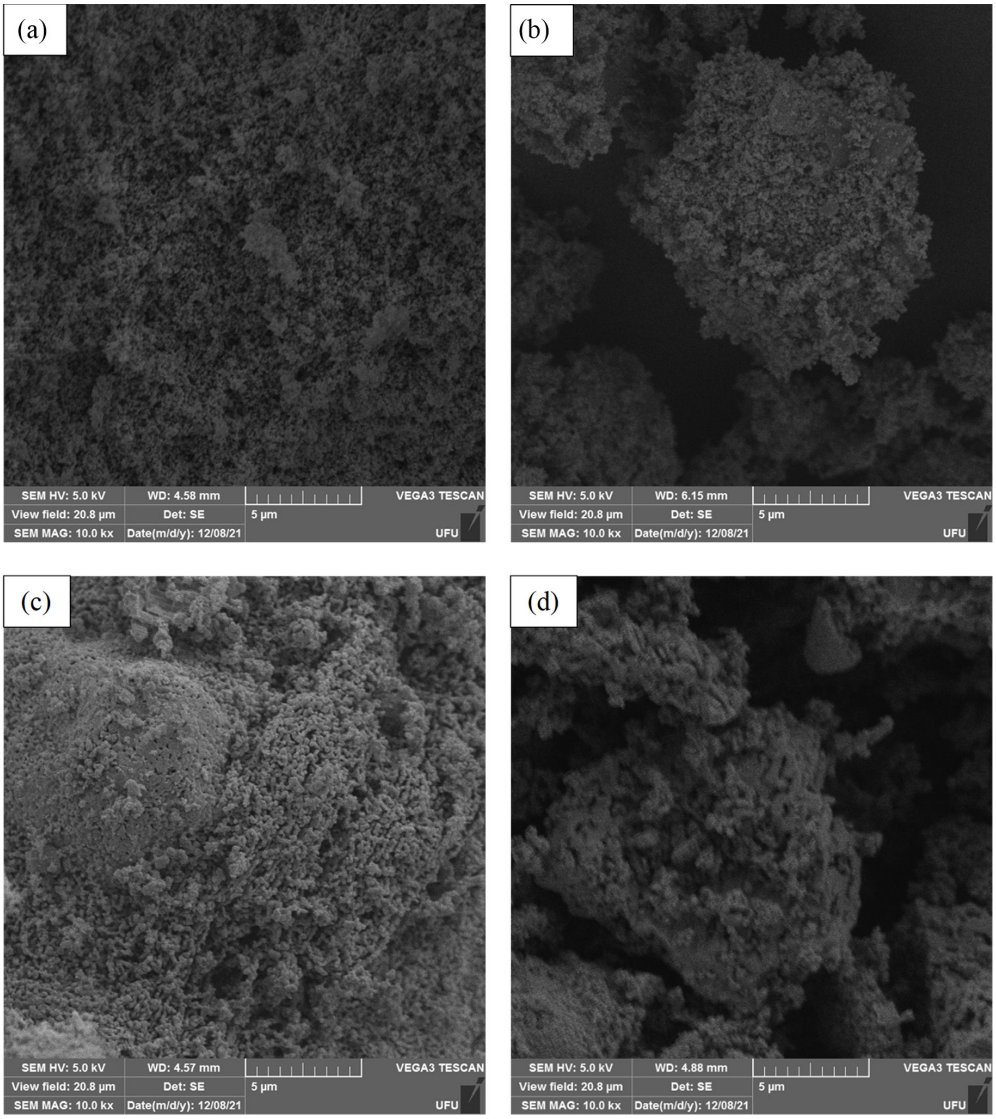

Figure 5. SEM images of the samples: (a) Nb_2O_5 A.H., (b) Nb_2O_5 A.C., (c) Nb_2O_5 commercial and (d) Nb_2O_5 C.H.

annealed (Nb_2O_5 A.C.), as can be seen in Figure 6. It can be observed that Nb_2O_5 A.H. sample is composed of a spherical agglomeration with size around 50 nm, formed by smaller particles with size around 10 nm. It can be observed two kinds of morphology, spherical and nanorod particles. The calcination of ammonium oxalate complex of niobium (Nb_2O_5 A.C.) resulted in the increase of the particles size (ca. 100 nm), due to the calcination process at high temperatures. It agrees with SEM images and specific surface area results. In Figure 6e is presented the high-resolution transmission electron microscopy (HRTEM) image of the Nb_2O_5 A.H. samples. It exhibits spherical and elongated particles with length size around 10 nm. This sample also presents interlayer distance of 0.37 nm, which is characteristic of the (001) plane of the pseudo-hexagonal crystalline phase of Nb_2O_5, according to XRD results.

XPS survey spectra confirmed the presence of Nb, O and C in both Nb_2O_5 surface samples (Figure S2a, SI section). Carbon peak located at 284.8 eV was used to calibrate the samples. In Figure S2b, the Nb 3d high-resolution XPS spectra show peaks at 207.6 and 210.3 eV, corresponding to Nb $3d_{3/2}$ and Nb $3d_{5/2}$ levels, respectively.[33,35,58] It confirms that both samples exhibit niobium in high valence (Nb^{5+}), as suggested by XRD and Raman spectroscopy results. The XPS results confirmed that it was not observed any segregation of metallic Nb at the surface of the sample.

Photocatalytic performance of Nb_2O_5 samples for organic pollutants degradation

The photocatalytic performance of the synthetized samples was investigated using two organic pollutants, Rhodamine B (dye) and amiloride (drug). Figure 7 shows the RhB photodegradation curves catalyzed by the

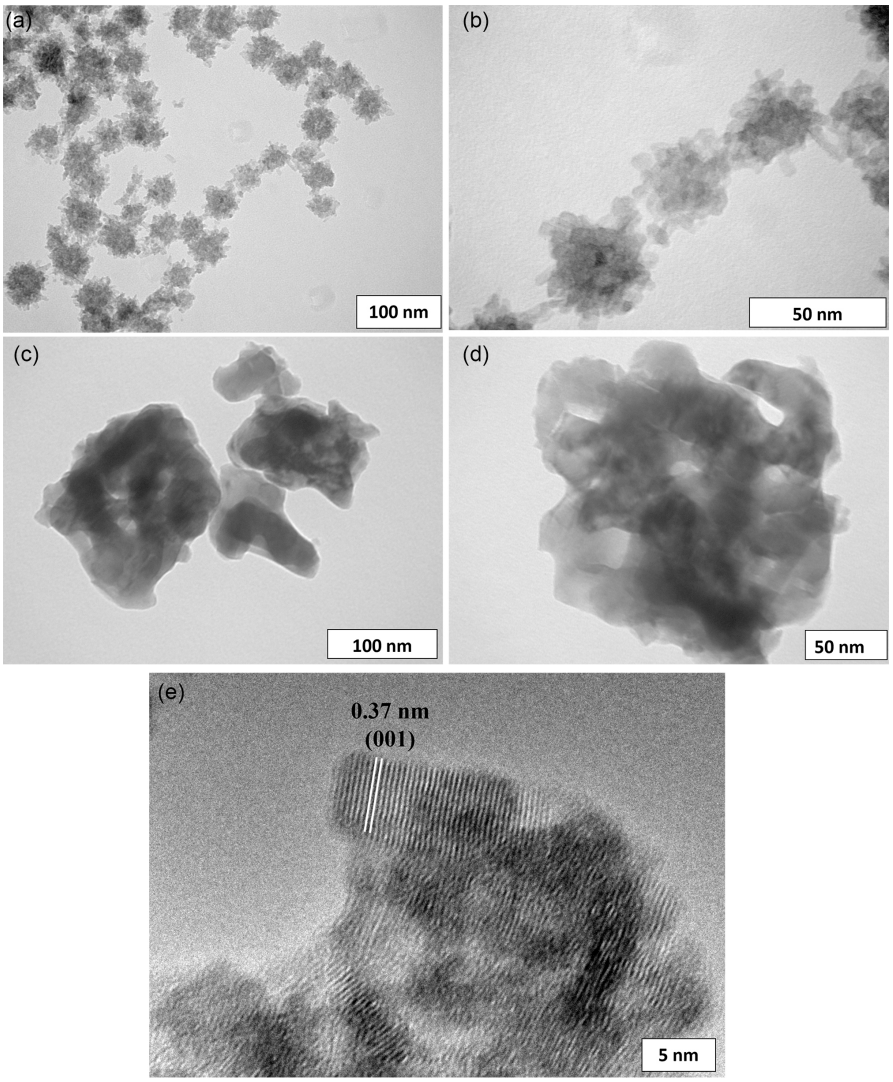

Figure 6. TEM images of the samples (a) and (b) Nb_2O_5 A.H., (c) and (d) Nb_2O_5 C.H., (e) HRTEM image of the Nb_2O_5 A.H.

Nb_2O_5 samples under UV radiation. The direct photolysis caused insignificant degradation of the dye. All the Nb_2O_5 were photoactive to promote the dye degradation. The photocatalytic performance of the synthetized samples was compared to the commercial Nb_2O_5. It can be observed that the hydrothermal treatment on commercial Nb_2O_5 precursor did not increase the photocatalytic activity of the Nb_2O_5 C.H., probably because the hydrothermal treatment did not cause any significant change in the sample's physical chemical properties. In addition, the precursor calcination of niobium ammonia complex presented a lower photocatalytic performance than the commercial Nb_2O_5. On the other hand, Nb_2O_5 A.H. showed an increased photoactivity in comparison to the reference sample. More than 60% of RhB was degraded after 180 min under UV irradiation. It can be concluded that Nb_2O_5 A.H. sample exhibited an increased photocatalytic activity due to the higher specific surface area and higher amount hydroxyl groups adsorbed on the surface of the material that may act as intermediaries on the hydroxyl radicals formation.[59] It is important to highlight that Nb_2O_5 samples exhibited different crystalline phases, and the observed order of photoactivity may be also related to the intrinsic activity of each crystalline phase.

For a better comprehension of the kinetic process and the photoactivity order, the photodegradation kinetics of the reaction was also studied. Through this study is possible to verify if the reaction follows the same mechanism during the evaluation time or if there was a change in the mechanism, in addition to verify if the different catalysts lead the reaction by the same mechanism.[48] Then, considering that the light source is constant and the number of active sites of the photocatalyst is dependent only on the superficial area and since no poisoning occurs during this process, it is expected that the reaction follows a first (equation 2) or second order kinetics (equation 3):

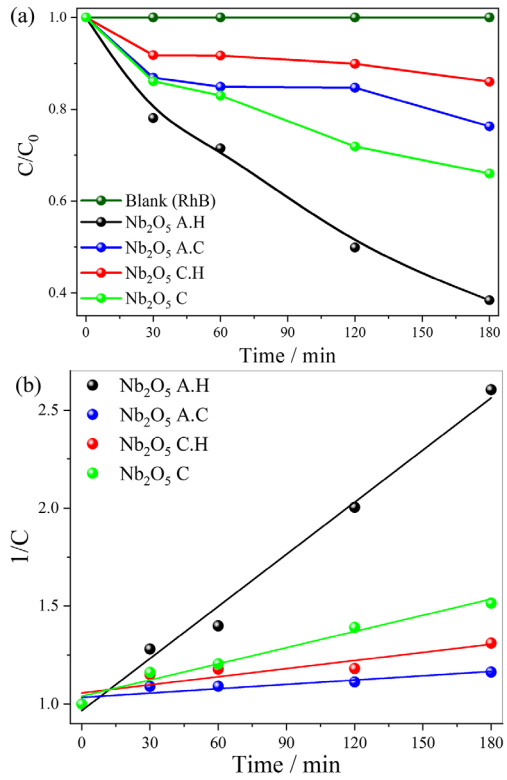

Figure 7. (a) Photodegradation curves of Rhodamine B (5 mg L^{-1}) catalyzed by the Nb_2O_5 samples under UV radiation; (b) second-order kinetics for the RhB degradation catalyzed by the Nb_2O_5 samples.

$$v = -\frac{d[RhB]}{dt} = k[RhB] \quad (2)$$

$$v = -\frac{d[RhB]}{dt} = k[RhB]^2 \quad (3)$$

where, v is the reaction rate; [RhB] is the dye concentration; t is the time and k is the rate constant. Integrating the velocity laws the following linear equations are obtained:

$$\ln\frac{[RhB]}{[RhB]_0} = -kt \quad (4)$$

$$\frac{[1]}{[RhB]} = \frac{[1]}{[RhB]_0} - k \quad (5)$$

The two linearized equations were applied to the data of RhB dye photodegradation kinetics. It was verified that the second-order kinetics presented a better fit to the experimental data than the first-order one. Therefore, the second-order rate constants are presented in Table 3, where the fitting is shown by the values of coefficient of determination (R^2), which corroborates the RhB photodegradation mechanism follows the second-order kinetics. The photoactivity order previously verified is confirmed by numerical values comparation of the rate constant obtained, where the sample Nb_2O_5 A.H. exhibited a k value 3 times higher than the commercial one.

Table 3. Rate constant of the RhB photodegradation reaction (k_{RhB}) and the coefficient of determination (R^2) for the Nb_2O_5 samples

Sample	$k_{RhB} \times 10^{-3}$ / min^{-1}	R^2
Nb_2O_5 A.H.	8.9	0.99
Nb_2O_5 A.C.	0.7	0.91
Nb_2O_5 C.H.	1.4	0.91
Nb_2O_5 C	2.7	0.98

To verify the versatility of the Nb_2O_5 samples for photocatalytic applications, they were applied to the amiloride photodegradation under ultraviolet radiation. Amiloride is a colorless organic pollutant; it is a drug extensively used for the treatment of hypertension, belonging to a class of pharmaceutical compounds that are often found in wastewater and can adversely affect water quality.[34] Figure 8 shows the amiloride photodegradation curves catalyzed by the Nb_2O_5 samples under UV radiation. All the samples were also active in the amiloride degradation. The Nb_2O_5 A.H. sample also showed a higher photocatalytic performance in comparison to the other samples, with 70% of drug degradation. The other samples were able to degrade only 50% after 120 min. The increased specific surface area and surface hydroxylation of Nb_2O_5 develop a key role in the photocatalytic activity of the samples for organic pollutant degradation. The importance of these parameters is closely related to the adsorption ability of the materials, since a higher specific surface area provides more active sites for molecule adsorption and can also affect the degradation mechanism via indirect or direct mechanism.[60,61]

The reaction mechanisms responsible for the pollutant's degradation were investigated by the photocatalytic essays

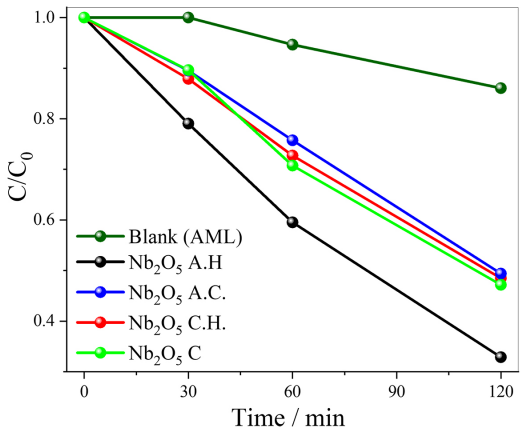

Figure 8. Photodegradation kinetics of amiloride (10 mg L^{-1}) catalyzed by the Nb_2O_5 samples under UV radiation.

in the presence of main active species scavengers, hydroxyl radical (•OH), superoxide radical ($O_2^{-\bullet}$) and photogenerated hole at valence band of the semiconductor. There are three main mechanisms that may be involved in the photocatalytic degradation process of pollutants: direct mechanism, indirect mechanism and photosensitization process.[59] Then, the degradation mechanism was investigated using the following main active species scavengers: 1-butanol (•OH scavenger), EDTA (h^+ scavenger) and benzoquinone ($O2^{-\bullet}$ scavenger).[62,63] The sample Nb_2O_5 A.H. was chosen to be applied in the study of the reaction mechanisms, because this sample presented the highest photoactivity, as observed by photodegradation experiments in Figures 7 and 8. Figure 9 shows that all scavengers employed promoted a decreasing in the photoactivity of the Nb_2O_5 A.H. sample. This is indicative that two radicalar species (•OH and $O_2^{-\bullet}$) and the hole photogenerated in the VB take part in the organic pollutant photodegradation. However, it can be observed that benzoquinone was the most efficient scavenger to decrease the photoactivity of Nb_2O_5 A.H. sample, which demonstrates that $O_2^{-\bullet}$ radical is the main radicalar species responsible for the organic pollutant photodegradation. Additionally, it can be observed that 1-butanol and EDTA caused similar reduction in the photocatalyst's activity, which means that the hole photogenerated in the VB did not present an important role, because it is just an intermediate in the formation of •OH radicals. Therefore, this result agrees that the indirect mechanism is the main responsible for the organic pollutant degradation, in agreement with a previous work of our group.[20]

Then, it can be proposed that photogenerated hole (h^+) at valence band of Nb_2O_5 could react with adsorbed water or hydroxyl group to produce hydroxyl radical (•OH). In the presence of dissolved oxygen, the photogenerated electron at conduction band (e^-) could be transferred to oxygen molecule, leading to the generation of superoxide radical ($O_2^{\bullet-}$) in the subsequent reaction.[56] The conduction band edge (E_{CB}) of Nb_2O_5 presents a more negative reduction potential than the oxygen molecule reduction potential, therefore, the electron transfer is spontaneous.[58,64]

The stability experiment (Figure 10) was performed under five cycles of photocatalytic experiment for RhB degradation using the Nb_2O_5 A.H. sample that presented the higher photoactivity (Figures 7 and 8). It can be observed that Nb_2O_5 A.H. sample shows a slight deviation in the efficiency through the five cycles, with a RhB dye degradation percentage ranging from 60 to 70%. However, it ultimately maintained constant efficiency across the five cycles, proving its reusability for several heterogeneous photocatalytic cycles.

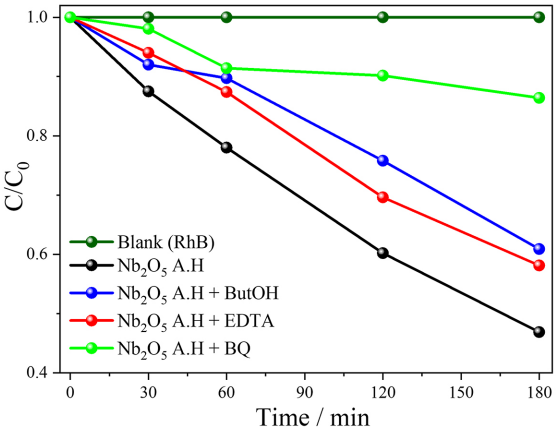

Figure 9. Photodegradation kinetics of RhB (5 mg L^{-1}) catalyzed by Nb_2O_5 A.H. samples in the presence of 1-butanol (100 µmol L^{-1}), EDTA and benzoquinone (50 µmol L^{-1}).

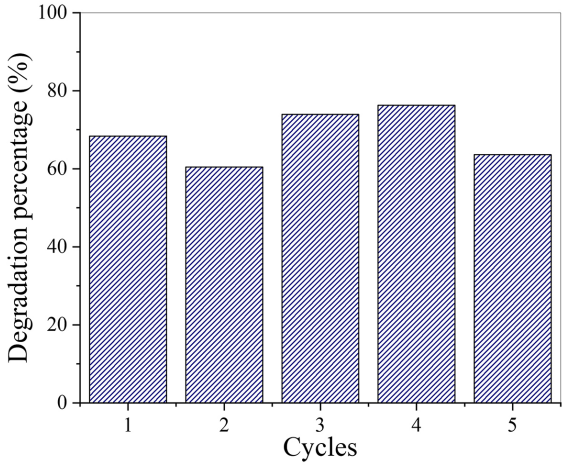

Figure 10. Stability of the Nb_2O_5 A.H. sample under five photocatalytic experiments cycles for RhB dye degradation.

Photocatalytic performance of Nb_2O_5 for H_2 production

The photodegradation mechanism results demonstrated that Nb_2O_5 A.H. sample exhibited the ability to produce $O_2^{-\bullet}$ radicals. It is an indicative that this sample is also able to promote the H_2 evolution reaction since the hydrogen formation exhibits a lower electrochemical reduction potential than the $O_2^{-\bullet}$ radicals formation. Therefore, Nb_2O_5 A.H. sample was employed as a photocatalyst to promote the H_2 evolution reaction, using 20% v/v methanol/water mixtures under UV-Vis light ($\lambda > 350$ nm). For comparison, Nb_2O_5 A.H. samples with and without Pt nanoparticles were also evaluated under the same conditions. The pristine Nb_2O_5 A.H. sample was not able to produce significative amounts of H_2; however, the Pt nanoparticles (1 wt.%) modified sample was photoactive to produce H_2, as can be seen in Figure 11. The low photoactivity of the pristine Nb_2O_5 A.H. sample can be related to the fast recombination of the photogenerated

electrons on conduction band of the semiconductor and due to the weak interaction between H^+ and photocatalyst surface. Then, the modification of the surface of the sample by Pt nanoparticles deposition can overcome both drawbacks. Pt is considered a cocatalyst and it is an excellent electron acceptor, which results in an increased charge carrier lifetime of the photocatalyst. Additionally, Pt can also act as proton reduction sites, due to its good interaction with H^+.[65,66] Nb_2O_5 A.H. modified with Pt was able to produce around 4 mmol g^{-1} of H_2 after 8 h of reaction. Our sample presented a similar result to Nb related compounds, for example, modified hexaniobate ($K_{4-x}H_xNb_6O_{17}$) with different cocatalysts, such as Co, Fe and Au.[37,67]

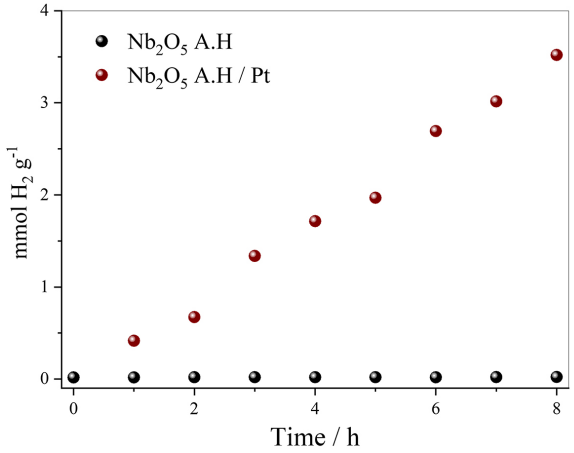

Figure 11. Photocatalytic hydrogen evolution from H_2O/methanol mixtures (20% v/v) catalyzed by Nb_2O_5 A.H. sample with and without Pt nanoparticles.

Conclusions

In summary, the synthesis method and the Nb precursor employed played an important role in the structural, morphologic, and surface properties of the Nb_2O_5 samples obtained. All samples were photoactive for organic pollutant photodegradation (Rhodamine B dye and amiloride drug). Nb_2O_5 sample obtained by hydrothermal method using ammonium niobium oxalate as Nb precursor exhibited the highest photocatalytic performance for RhB dye and amiloride drug degradation because this sample has the smaller particle size, higher specific surface area and concentration of hydroxyl groups on the surface. The photodegradation mechanism evaluation showed that indirect mechanism mediated by radicalar species ($O_2^{-\bullet}$ and $OH^{\bullet}$) was the main responsible for the organic pollutant degradation. The modification of Nb_2O_5 with Pt resulted in a material with good performance for H_2 production. Therefore, Nb_2O_5 is a semiconductor with excellent photocatalytic properties to be applied in water effluent treatment (organic pollutants photodegradation) and for renewable energy production (H_2 production).

Supplementary Information

Supplementary data are available free of charge at http://jbcs.sbq.org.br as PDF file.

Acknowledgments

The authors acknowledge FAPEMIG (Minas Gerais Research Foundation, grant: APQ-00282-21, BPD-00811-22, BPD-00165-22 and RED-00175-22) and CNPq (Brazilian National Council for Scientific and Technological Development, grants: 407497/2018-8, 405819/2022-6 and 150371/2023-3) for the financial support. The authors thank to GMIT group and MSc Lucas Leão (UFU) for N_2 physisorption measurements. O. F. Lopes also acknowledges Alexander von Humboldt Foundation by Return Fellowship Grant.

Author Contributions

Marlete A. Souza was responsible for investigation, methodology, writing original draft; Marcela P. Bernardo for formal analysis, investigation, writing original draft; Higor O. Alves for formal analysis, investigation; Cleiton P. M. da Silva for investigation, methodology; Antonio Otavio Patrocinio for funding acquisition, resources, writing-original draft, review and editing; Osmando Lopes for conceptualization, funding acquisition, project administration, resources, supervision, writing-original draft, review and editing.

References

1. Yaseen, M.; Khan, A.; Humayun, M.; Farooq, S.; Shah, N.; Bibi, S.; Khattak, Z. A. K.; Rehman, A. U.; Ahmad, S.; Ahmad, S. M.; Bououdina, M.; Ullah, H.; *Macromol. Mater. Eng.* **2023**, *308*, 2200695. [Crossref]
2. Chaves, M. J. S.; Barbosa, S. C.; Primel, E. G.; Castro, Í. B.; *J. Braz. Chem. Soc.* **2023**, *34*, 276. [Crossref]
3. Sharma, K.; Dutta, V.; Sharma, S.; Raizada, P.; Hosseini-Bandegharaei, A.; Thakur, P.; Singh, P.; *J. Ind. Eng. Chem.* **2019**, *78*, 1. [Crossref]
4. Saad, I.; Ralha, N.; Abukhadra, M. R.; Al Zoubi, W.; Ko, Y. G.; *J. Water Process Eng.* **2023**, *52*, 103572. [Crossref]
5. Teixeira, I. F.; Quiroz, J.; Homsi, M. S.; Camargo, P. H. C.; *J. Braz. Chem. Soc.* **2020**, *31*, 211. [Crossref]
6. Gonçalves, H. B.; Freitas, D. V.; Souza, E. J.; Melo, M. A.; Gonzalez-Moya, J. R.; Padrón-Hernández, E.; Khan, S.; Machado, G.; *J. Braz. Chem. Soc.* **2022**, *33*, 894. [Crossref]

7. Bueno, R. T.; Lopes, O. F.; Carvalho, K. T. G.; Ribeiro, C.; Mourão, H. A. J. L.; *Quim. Nova* **2019**, *42*, 661. [Crossref]
8. Macedo, G. K.; Dias, E. H.; Ribeiro, C.; Lopes, O. F.; *J. Braz. Chem. Soc.* **2022**, *33*, 948. [Crossref]
9. Silva, F. B. F.; da Silva, G. T. S. T.; Torres, J. A.; Ribeiro, C.; *J. Braz. Chem. Soc.* **2022**, *33*, 725. [Crossref]
10. Aiempanakit, M.; Sangkaworn, J.; Worawannotai, N.; Laohhasurayotin, K.; Sangchay, W.; Laksee, S.; Suwanchawalit, C.; *J. Braz. Chem. Soc.* **2022**, *33*, 541. [Crossref]
11. da Silva, E. C.; de Moraes, M. O. S.; Brito, W. R.; Passos, R. R.; Brambilla, R. F.; da Costa, L. P.; Pocrifka, L. A.; *J. Braz. Chem. Soc.* **2020**, *31*, 1648. [Crossref]
12. Lopes, O. F.; de Mendonça, V. R.; Umar, A.; Chuahan, M. S.; Kumar, R.; Chauhan, S.; Ribeiro, C.; *New J. Chem.* **2015**, *39*, 4624. [Crossref]
13. Carvalho, K. T. G.; Fidelis, S. C.; Lopes, O. F.; Ribeiro, C.; *Ceram. Int.* **2015**, *41*, 10587. [Crossref]
14. de Almeida, J. C.; Correâ, M. T.; Koga, R. H.; Del Duque, D. M. S.; Lopes, O. F.; da Silva, G. T. S. T.; Ribeiro, C.; de Mendonçą, V. R.; *New J. Chem.* **2020**, *44*, 18216. [Crossref]
15. Yan, J.; Wu, G.; Guan, N.; Li, L.; *Appl. Catal., B* **2014**, *152-153*, 280. [Crossref]
16. Clabel H, J. L.; Chacaliaza-Ricaldi, J.; Marega Jr., E.; *Front. Nanotechnol.* **2022**, *4*, 827925. [Crossref]
17. Tasleem, S.; Tahir, M.; *Renewable Sustainable Energy Rev.* **2020**, *132*, 110073. [Crossref]
18. Nunes, B. N.; Lopes, O. F.; Patrocinio, A. O. T.; Bahnemann, D. W.; *Catalysts* **2020**, *10*, 126. [Crossref]
19. Rodrigues, T. A.; Falsetti, P. H. E.; Del Duque, D. M. S.; da Silva, G. T. S. T.; Lopes, O. F.; Avansi, W.; Ribeiro, C.; de Mendonça, V. R.; *ChemCatChem* **2021**, *13*, 730. [Crossref]
20. Lopes, O. F.; Paris, E. C.; Ribeiro, C.; *Appl. Catal., B* **2014**, *144*, 800. [Crossref]
21. Lopes, O. F.; de Mendonca, V. R.; Silva, F. B. F.; Paris, E. C.; Ribeiro, C.; *Quim. Nova* **2015**, *38*, 106. [Crossref]
22. Nico, C.; Monteiro, T.; Graça, M. P. F.; *Prog. Mater. Sci.* **2016**, *80*, 1. [Crossref]
23. Rani, R. A.; Zoolfakar, A. S.; O'Mullane, A. P.; Austin, M. W.; Kalantar-Zadeh, K.; *J. Mater. Chem. A* **2014**, *2*, 15683. [Crossref]
24. Su, K.; Liu, H.; Gao, Z.; Fornasiero, P.; Wang, F.; *Adv. Sci.* **2021**, *8*, 2003156. [Crossref]
25. Su, K.; Wang, Y.; Zhang, C.; Gao, Z.; Han, J.; Wang, F.; *Appl. Catal., B* **2021**, *298*, 120554. [Crossref]
26. Bhalla, A. S.; Guo, R.; Roy, R.; *Mater. Res. Innovations* **2000**, *4*, 3. [Crossref]
27. Guo, W.; Bo, C.; Li, W.; Feng, Z.; Cong, E.; Yang, L.; Yang, L.; *Nanomaterials* **2022**, *12*, 1690. [Crossref]
28. Ücker, C. L.; Goetzke, V.; Riemke, F. C.; Oliveira, M. E.; Carreno, N. L. V.; Morisso, F. D. P.; Teodoro, M. D.; Mastelaro, V. R.; Moreira, M. L.; Raubach, C. W.; Cava, S. S.; *J. Photochem. Photobiol., A* **2023**, *435*, 114294. [Crossref]
29. Cui, H.; Dwight, K.; Soled, S.; Wold, A.; *J. Solid State Chem.* **1995**, *115*, 187. [Crossref]
30. Peng, C.; Xie, X.; Xu, W.; Zhou, T.; Wei, P.; Jia, J.; Zhang, K.; Cao, Y.; Wang, H.; Peng, F.; Yang, R.; Yan, X.; Pan, H.; Yu, H.; *Chem. Eng. J.* **2021**, *421*, 128766. [Crossref]
31. Zhao, W.; Zhao, W.; Zhu, G.; Lin, T.; Xu, F.; Huang, F.; *Dalton Trans.* **2016**, *45*, 3888. [Crossref]
32. Leite, E. R.; Vila, C.; Bettini, J.; Longo, E.; *J. Phys. Chem. B* **2006**, *110*, 18088. [Crossref]
33. da Silva, G. T. S. T.; Nogueira, A. E.; Oliveira, J. A.; Torres, J. A.; Lopes, O. F.; Ribeiro, C.; *Appl. Catal., B* **2019**, *242*, 349. [Crossref]
34. Carvalho, K. T. G.; Lopes, O. F.; Ferreira, D. C.; Ribeiro, C.; *J. Alloys Compd.* **2019**, *797*, 1299. [Crossref]
35. da Silva, G. T. S. T.; Carvalho, K. T. G.; Lopes, O. F.; Ribeiro, C.; *Appl. Catal., B* **2017**, *216*, 70. [Crossref]
36. Nunes, B. N.; Patrocinio, A. O. T.; Bahnemann, D. W.; *J. Phys.: Condens. Matter* **2019**, *31*, 394001. [Crossref]
37. Alves, H. O.; Frachoni, B. S. D.; Nunes, B. N.; Teixeira, P. R.; Paniago, R. M.; Bahnemann, D. W.; Paterno, L. G.; Patrocinio, A. O. T.; *ACS Appl. Energy Mater.* **2022**, *5*, 8371. [Crossref]
38. Chen, Y.-C.; Hsu, Y. K.; Popescu, R.; Gerthsen, D.; Lin, Y. G.; Feldmann, C.; *Nat. Commun.* **2018**, *9*, 232. [Crossref]
39. Leal, G. F.; Lima, S.; Graça, I.; Carrer, H.; Barrett, D. H.; Teixeira-Neto, E.; Curvelo, A. A. S.; Rodella, C. B.; Rinaldi, R.; *iScience* **2019**, *15*, 467. [Crossref]
40. Ventura, W. M.; Batalha, D. C.; Fajardo, H. V.; Taylor, J. G.; Marins, N. H.; Noremberg, B. S.; Ta, T.; Carreño, N. L. V.; *Catal. Commun.* **2017**, *99*, 135. [Crossref]
41. da Cruz, J. A.; Volnistem, E. A.; Ferreira, R. F.; Freitas, D. B.; Sales, A. J. M.; Costa, L. C.; Graça, M. P. F.; *Therm. Sci. Eng. Prog.* **2021**, *25*, 101015. [Crossref]
42. Zhou, K. G.; Tokuda, M.; *J. Cent. South Univ. Technol.* **2000**, *7*, 173. [Crossref]
43. Pilarek, B.; Pelczarska, A. J.; Szczygieł, I.; *J. Therm. Anal. Calorim.* **2017**, *130*, 77. [Crossref]
44. Xue, J.; Wang, R.; Zhang, Z.; Qiu, S.; *Dalton Trans.* **2016**, *45*, 16519. [Crossref]
45. Weissman, J. G.; Ko, E. I.; Wynblatt, P.; Howe, J. M.; *Chem. Mater.* **1989**, *1*, 187. [Crossref]
46. Gomes, G. H. M.; Mohallem, N. D. S.; *Mater. Lett.* **2022**, *318*, 132136. [Crossref]
47. Gomes, G. H. M.; de Andrade, R. R.; Mohallem, N. D. S.; *Micron* **2021**, *148*, 103112. [Crossref]
48. de Mendonça, V. R.; Ribeiro, C.; *Appl. Catal., B* **2011**, *105*, 298. [Crossref]
49. Rychtowski, P.; Tryba, B.; Skrzypska, A.; Felczak, P.; Sreńscek-Nazzal, J.; Wróbel, R. J.; Nishiguchi, H.; Toyoda, M.; *Catalysts* **2022**, *12*, 386. [Crossref]

50. Hussain, M.; Bensaid, S.; Geobaldo, F.; Saracco, G.; Russo, N.; *Ind. Eng. Chem. Res.* **2011**, *50*, 2536. [Crossref]
51. Brayner, R.; Bozon-Verduraz, F.; *Phys. Chem. Chem. Phys.* **2003**, *5*, 1457. [Crossref]
52. Jehng, J.-M.; Wachs, I. E.; *Chem. Mater.* **1991**, *3*, 100. [Crossref]
53. Ücker, C. L.; Gularte, L. T.; Fernandes, C. D.; Goetzke, V.; Moreira, E. C.; Raubach, C. W.; Moreira, M. L.; Cava, S. S.; *J. Am. Ceram. Soc.* **2019**, *102*, 1884. [Crossref]
54. Ücker, C. L.; Riemke, F. C.; de Andrade Neto, N. F.; Santiago, A. A. G.; Siebeneichler, T. J.; Carreño, N. L. V.; Moreira, M. L.; Raubach, C. W.; Cava, S.; *Chem. Phys. Lett.* **2021**, *764*, 138271. [Crossref]
55. Xie, J.; Cao, Y.; Jia, D.; *J. Alloys Compd.* **2020**, *832*, 154953. [Crossref]
56. Wolski, L.; Walkowiak, A.; Ziolek, M.; *Mater. Res. Bull.* **2019**, *118*, 110530. [Crossref]
57. Dalmaschio, C. J.; Ribeiro, C.; Leite, E. R.; *Nanoscale* **2010**, *2*, 2336. [Crossref]
58. Wang, L.; Li, Y.; Han, P.; *Sci. Rep.* **2021**, *11*, 22950. [Crossref]
59. de Mendonça, V. R.; Lopes, O. F.; Fregonesi, R. P.; Giraldi, T. R.; Ribeiro, C.; *Appl. Surf. Sci.* **2014**, *298*, 182. [Crossref]
60. Qiao, D.; Li, Z.; Duan, J.; He, X.; *Chem. Eng. J.* **2020**, *400*, 125952. [Crossref]
61. Chen, J.; Xiong, Y.; Duan, M.; Li, X.; Li, J.; Fang, S.; Qin, S.; Zhang, R.; *Langmuir* **2020**, *36*, 520. [Crossref]
62. Li, Y.; Wang, J.; Yao, H.; Dang, L.; Li, Z.; *J. Mol. Catal. A: Chem.* **2011**, *334*, 116. [Crossref]
63. Cao, J.; Xu, B.; Luo, B.; Lin, H.; Chen, S.; *Catal. Commun.* **2011**, *13*, 63. [Crossref]
64. Hong, Y.; Li, C.; Zhang, G.; Meng, Y.; Yin, B.; Zhao, Y.; Shi, W.; *Chem. Eng. J.* **2016**, *299*, 74. [Crossref]
65. Wang, S.; Cui, D.; Hao, W.; Du, Y.; *Energy Fuels* **2022**, *36*, 11394. [Crossref]
66. Yang, J.; Wang, D.; Han, H.; Li, C.; *Acc. Chem. Res.* **2013**, *46*, 1900. [Crossref]
67. Nunes, B. N.; Bahnemann, D. W.; Patrocinio, A. O. T.; *ACS Appl. Energy Mater.* **2021**, *4*, 3681. [Crossref]

Submitted: April 30, 2023
Published online: October 20, 2023